Hydrogen Bonding Pathways in Human Dihydroorotate Dehydrogenase

Yolanda A. Small,[†] Victor Guallar,[‡,§] Alexander V. Soudackov,[†] and Sharon Hammes-Schiffer*[,†]

Department of Chemistry, 104 Chemistry Building, Pennsylvania State University, University Park, Pennsylvania 16802, Department of Biochemistry and Molecular Biophysics, 700 South Euclid Avenue, Room 112, Campus Box 8036, Washington University, St. Louis, Missouri 63110, and Barcelona Supercomputing Center, Jordi Girona 31, 08034 Barcelona, Spain

Received: August 4, 2006

Dihydroorotate dehydrogenase (DHOD) catalyzes the only redox reaction in the pathway for pyrimidine biosynthesis. In this reaction, a proton is transferred from a carbon atom of the substrate to a serine residue, and a hydride is transferred from another carbon atom of the substrate to a cofactor. The deprotonation of the substrate is postulated to involve a proton relay mechanism along a hydrogen bonding pathway in the active site. In this paper, molecular dynamics simulations are used to identify and characterize potential hydrogen bonding pathways that could facilitate the redox reaction catalyzed by human DHOD. The observed pathways involve hydrogen bonding of the active base serine to a water molecule, which is hydrogen bonded to the substrate carboxylate group or a threonine residue. The threonine residue is positioned to enable proton transfer to another water molecule leading to the bulk solvent. The impact of mutating the active base serine to cysteine is also investigated. This mutation is found to increase the average donor−acceptor distances for proton and hydride transfer and to disrupt the hydrogen bonding pathways observed for the wild-type enzyme. These effects could lead to a significant decrease in enzyme activity, as observed experimentally for the analogous mutant in *Escherichia coli* DHOD.

I. Introduction

Dihydroorotate dehydrogenase (DHOD) catalyzes the only redox reaction in the pathway for pyrimidine biosynthesis. In this reaction, dihydroorotate (DHO) is oxidized to orotate (ORO) by the enzyme-bound flavin mononucleotide (FMN). Specifically, the C5 pro-*S* hydrogen of DHO is removed as a proton by an enzymatic base, and the C6 hydrogen of DHO is transferred as a hydride to the isoalloxazine ring of the flavin.[1−3] Pyrimidines are required for the supply of precursors for RNA and DNA synthesis. The diversity among DHODs of different organisms[4] enables the development of compounds that selectively inhibit pyrimidine biosynthesis in some organisms while not affecting others. As a result, these enzymes are promising targets for treating cancer, malaria, gastric ulcers, and rheumatoid arthritis.[5−8] One prominent example is the immunosuppressive drug leflunomide, which inhibits human DHOD and has been used in the clinical treatment of rheumatoid arthritis.[7,9,10]

DHOD enzymes have been divided into two classes on the basis of sequence homology.[11] Class 1 enzymes are soluble, located in the cytosol, and found in Gram-positive bacteria and some lower eukaryotes. Class 2 enzymes are associated with cell membranes and are found in most eukaryotes and Gram-negative bacteria. Class 1 is further divided into 1A and 1B. The 1A enzymes are thought to use fumarate to reoxidize the flavin. In contrast, the reoxidation of the flavin in the 1B enzymes is thought to involve a series of oxidizing reactions involving an iron−sulfur center and other cofactors. The class 2 enzymes are thought to use ubiquinone to reoxidize the flavin. An important distinction is that class 1 enzymes use cysteine as the active site base for deprotonation of the substrate, while class 2 enzymes use serine for this purpose.[1,3,12−14] The kinetics of the hydride and proton transfer reactions in the class 1A, 1B, and 2 enzymes have been studied extensively.[13,15−18] Structures have been determined for the class 1A and 1B enzymes from *Lactococcus lactis*[1,2,4,19] and the class 2 enzyme from rat,[20] human,[3] and *E. coli*.[14] The structures are all similar at the orotate binding site except for the active site base.

The present study focuses on human DHOD, which is a class 2 enzyme. The X-ray crystallographic structure of human DHOD[3] suggests that the catalytic base, Ser215, is hydrogen bonded to a tightly bound water molecule, which in turn is hydrogen bonded to Thr218. Both Ser215 and Thr218 are conserved in class 2 DHODs. Typically, serine does not play the role of a catalytic base in enzymatic catalysis. Hydrogen bonding in the active site could enhance the basicity of Ser215, however, thereby facilitating the deprotonation of the substrate. Moreover, deprotonation of the substrate could involve a proton relay mechanism along a hydrogen bonding pathway in the active site. Although cysteine plays the role of the catalytic base in class 1 DHOD enzymes, mutagenesis of the active serine residue to cysteine was found to reduce the enzyme activity 4-fold in human DHOD[21] and 500-fold in *E. coli* DHOD.[11]

In this paper, we use computational methods to investigate potential proton relay pathways in the active site of human DHOD. In addition to studying wild-type (WT) human DHOD, we also study the mutant enzyme in which Ser215 is replaced by cysteine. Despite the biological importance of this enzyme, there have not been any previous molecular dynamics studies on DHOD, although similar hydrogen bonding analyses have

* Corresponding author. E-mail: shs@chem.psu.edu.
[†] Pennsylvania State University.
[‡] Washington University.
[§] Barcelona Supercomputing Center.

10.1021/jp065034t CCC: $33.50
Published on Web 09/12/2006

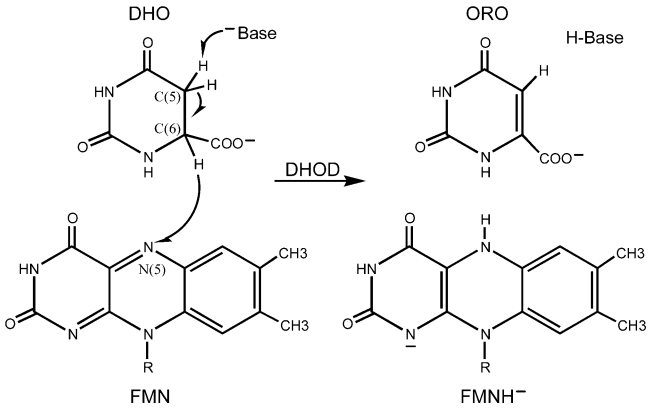

Figure 1. The proton and hydride transfer reactions catalyzed by DHOD. The substrate DHO is oxidized to ORO, and the cofactor FMN is reduced. The base is cysteine in class 1 DHOD enzymes and serine in class 2 DHOD enzymes.

been performed for other enzymes.[22−25] An outline of the paper is as follows: Section II describes the computational methods, section III presents the results and analysis, and the final section summarizes the conclusions.

II. Methods

The starting coordinates were obtained from the X-ray crystallographic structure for human DHOD (PDB code 1D3G).[3] In this crystal structure, the product ORO is bound to the enzyme, and the cofactor FMN is in the reactant oxidized form. The crystal structure includes the substrate and cofactor, 396 resolved residues, 274 resolved crystallographic water molecules, and seven unresolved residues that were filled using side-chain sampling and the rotamer library in the JACKAL suite of programs.[26] JACKAL was also used to add hydrogens to the protein and to determine the residue protonation states based on the local hydrogen bonding networks. Hydrogens were added to the substrate and cofactor to model the reactant state of the enzyme, in which the substrate is DHO and the cofactor is oxidized FMN, as depicted in Figure 1. All of the hydrogen coordinates were optimized with IMPACT[27] using the OPLS-2001 force field.[28]

The substrate and cofactor geometries for the reactant state were optimized with QSite[29] using a mixed quantum mechanical/molecular mechanical (QM/MM) method.[30] In these calculations, the substrate and cofactor were treated quantum mechanically at the B3LYP/6-31G** level,[31−35] and the remaining residues and crystallographic waters were treated with the OPLS-2001 force field.[28] The coordinates of the protein residues and crystallographic waters were fixed during the optimization of the substrate and cofactor. After this optimization, the Ser215Cys mutant enzyme was generated by replacing the serine with cysteine (i.e., replacing the oxygen with sulfur).

We performed calculations on both the WT DHOD and the Ser215Cys mutant DHOD enzymes. Both enzymes were solvated with simple-point-charge (SPC) water molecules[36] in a periodically replicated cubic box with sides of length 70 Å. The nonzero charge of +10 on the system was neutralized by converting solvent molecules near positively charged residues on the periphery of the enzyme to negatively charged chloride ions. Note that these chloride anions were more than 15 Å from the active site. To ensure a smooth transition from the structures obtained with the QM/MM calculations, which used the OPLS-2001 force field, the system was first equilibrated with IMPACT[27] using the OPLS-2001 force field.[28] The charges for the substrate and cofactor were determined with the electrostatic potential (ESP) method in QSite.[37−39] The temperature was maintained with a Berendsen thermostat,[40] and the long-range electrostatic interactions were treated with the Ewald method.[41] The coordinates of the substrate and cofactor were fixed to the QM/MM optimized values during the equilibration of the enzyme and solvent. In the initial preparation of the system, the enzyme was fixed, and the solvent was minimized with the steepest descent method for 200 steps. Then the enzyme backbone was fixed, and the solvent, hydrogen atoms of the enzyme, and side chains of the enzyme were minimized with the steepest descent method for another 200 steps. Finally, all atoms in the system were minimized with the steepest descent method for 200 steps and with the conjugate gradient method for 300 steps.

After this initial preparation of the system, three phases of molecular dynamics were performed. In each phase, the system was slowly heated in increments of 50 K from 0 to 300 K for 2 ps at each temperature, run at 300 K for 40 ps, and then slowly cooled in increments of 50 K from 250 to 0 K for 2 ps at each temperature. New velocities were generated from a Boltzmann distribution at each temperature. The substrate and cofactor were fixed at the QM/MM optimized values throughout this simulated annealing process. In phase I, only the solvent and hydrogen atoms were unconstrained. In phase II, the solvent, hydrogen atoms, and residues within 3 Å of the substrate were unconstrained. In phase III, the solvent and all enzyme residues were unconstrained.

The trajectories used for the hydrogen bonding analysis were generated with the GROMACS molecular dynamics package.[42,43] For these simulations, we used the GROMACS force field[42,43] with the particle mesh Ewald method[44] for long-range electrostatic interactions. To be consistent with the GROMACS force field, the charges on the substrate and cofactor were determined with the method described in ref 45. The protein, substrate, cofactor, and solvent were each separately coupled to Nose-Hoover thermostats[46,47] to maintain the temperature. The SHAKE algorithm[48] was used to constrain all of the X−H bonds throughout the simulation. The time step for these simulations was 1 fs.

Starting with the final structure from the simulated annealing procedure, the system was equilibrated with GROMACS to account for the differences in force fields. First, a slow heating in 50 K increments for 2 ps at each temperature from 0 to 300 K was performed with the coordinates of the substrate and cofactor fixed to the QM/MM optimized values. Starting with the final structure from this procedure, four independent trajectories were initiated at 300 K by choosing random velocities from a Boltzmann distribution. In these trajectories, the substrate and cofactor were no longer fixed to the QM/MM optimized values. The distance between the center of mass of the proton and hydride donor atoms and the proton acceptor was constrained to the initial values using the SHAKE algorithm[48] for the first 300 ps of molecular dynamics to prevent drifting. Then this constraint was removed, and the system was further equilibrated with an additional 300 ps of molecular dynamics. After this equilibration procedure, we generated 1 ns of molecular dynamics data for each independent trajectory, leading to 4 ns of data for the WT enzyme and 4 ns of data for the Ser215Cys mutant enzyme.

III. Results

We calculated the root-mean-square deviation (RMSD) of the α carbons relative to the crystal structure for all of the trajectories. The average RMSD over the four 1-ns trajectories

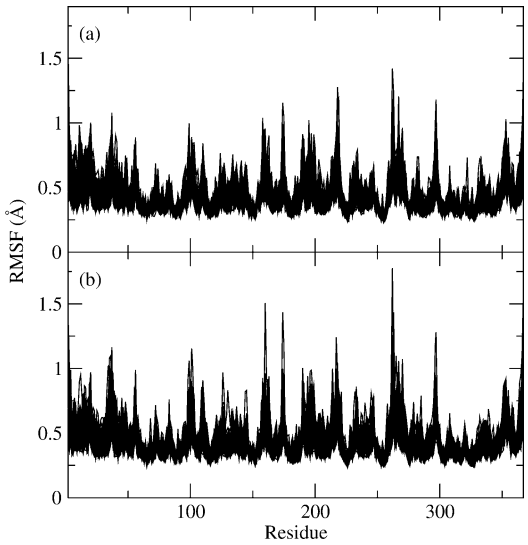

Figure 2. Root-mean-square fluctuations of the C_α atoms with respect to the average values for a representative (a) WT trajectory and (b) Ser215Cys mutant trajectory.

is 1.56 Å for the WT enzyme and 1.66 Å for the mutant enzyme. We also calculated the time-averaged root-mean-square fluctuation (RMSF) per residue. Figure 2 depicts the RMSF for representative WT and mutant trajectories. As expected, the most flexible residues are located near the surface of the protein, whereas the hydrophobic core of the protein maintains a relatively rigid structure. The similarity of the RMSF for the WT and mutant enzymes suggests that the mutation does not cause major structural rearrangements.

We monitored the distance between the donor and acceptor atoms for the proton and hydride transfer reactions involving the substrate. For the WT enzyme, the average proton donor−acceptor distance is 3.55 ± 0.36 Å, and the average hydride donor−acceptor distance is 3.68 ± 0.27 Å. For the mutant enzyme, the average proton donor−acceptor distance is 4.25 ± 0.36 Å, and the average hydride donor−acceptor distance is 4.18 ± 0.12 Å. Although these average donor−acceptor distances are too large for hydrogen transfer, thermal fluctuations of the system lead to sampling of smaller distances that enable proton and hydride transfer. The greater average donor−acceptor distances for the mutant are consistent with the significantly lower activity of the mutant enzyme. The greater proton donor−acceptor distance for the mutant may arise from the larger van der Waals radius of the sulfur atom in cysteine compared to that of the oxygen atom in serine.

TABLE 1: Percentage of Time That Each Hydrogen Bonding Pathway Was Observed for Each of the Four Independent WT Trajectories[a]

	traj 1	traj 2	traj 3	traj 4
water present	100	99	93	100
carboxylate path	98	0.79	87	73
threonine path	0.019	93	0.05	1.8
dual path	0.022	0.14	0.17	22

[a] The WT hydrogen bonding pathways are depicted in Figure 4; the percentage of time that a water molecule is present in the active site cavity, as defined in the text, is also given.

We also monitored the geometry and orientation of the substrate. Figure 3 depicts two distinct substrate conformations that have different values of the angle α involving the carboxylate carbon atom and two ring atoms. For the WT trajectories, the average value of the angle α is (158 ± 2)°. Moreover, a water molecule remains near Ser215 in all of the WT trajectories. In three of the four mutant trajectories, however, the carboxylate group of the substrate bends toward the cysteine base, so the average angle α is (111 ± 4)°, and the nearby water molecule is expelled. The larger van der Waals radius of the sulfur atom may induce the expulsion of the water molecule, which in turn may cause the carboxylate to bend toward the cysteine base to stabilize the negative charge on the carboxylate through hydrogen bonding. The bent substrate conformation and absence of the nearby water molecule widens the cavity in the vicinity of the cysteine residue. This widening may cause the interruption of the network of hydrogen bonds that are critical for the proton relay pathway and hence may contribute to the reduction in the mutant activity.

To assist in our analysis of hydrogen bonding pathways, we quantified the presence of a water molecule in the active site cavity. For this purpose, we defined a sphere of radius 3.3 Å centered at the center of mass of the oxygen atoms on Ser215, Thr218, and the carboxylate group of the substrate. The percentage of time that a water molecule is found in this sphere for each trajectory is given in Table 1. For the WT trajectories, a water molecule is present in the active site cavity virtually 100% of the time for three of the trajectories and 93% of the time for the other trajectory. For the mutant trajectories, a water molecule is absent from the active site cavity virtually 100% of the time for three of the trajectories and is present 100% of the time for the other trajectory. For the mutant trajectory with a water molecule in the active site cavity, the water molecule hydrogen bonds to Thr218 5% of the time, to the carboxylate group of the substrate 10% of the time, and to both Thr218 and

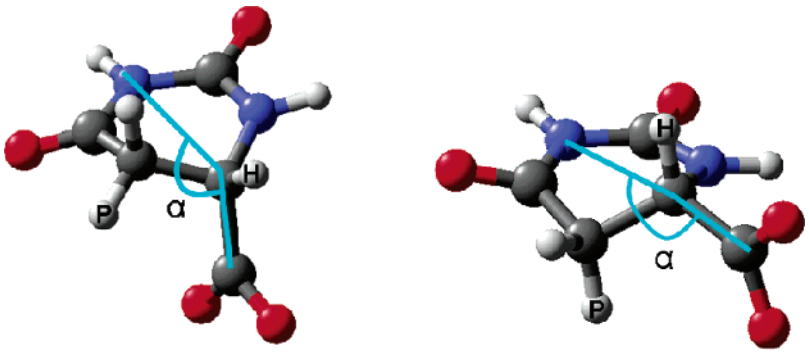

α = 111° α = 158°

Figure 3. The two dominant conformations of the substrate DHO observed in the Ser215Cys mutant (left) and the WT (right) trajectories. The transferring proton is labeled as P, and the transferring hydride is labeled as H.

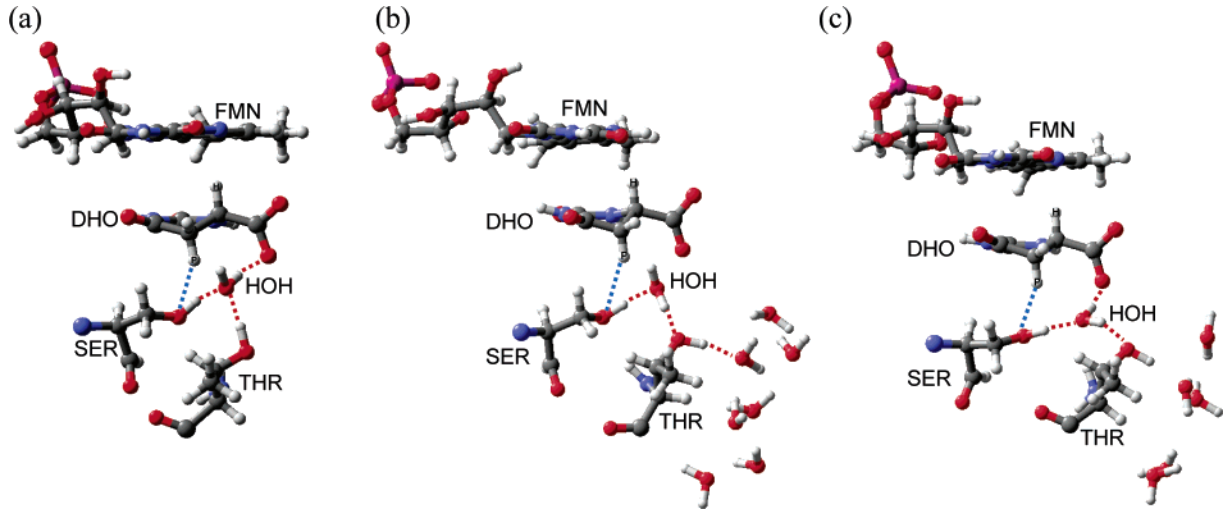

Figure 4. Hydrogen bonding pathways observed in the WT trajectories: (a) carboxylate pathway; (b) threonine pathway; (c) dual pathway. The transferring proton is labeled as P, and the transferring hydride is labeled as H.

the carboxylate group 4% of the time. This water molecule does not participate in the complete hydrogen bonding pathways discussed below, however, because Cys215 is too far away from the water molecule.

A proton relay mechanism has been hypothesized to facilitate the proton-transfer reaction from the substrate to Ser215. To gain insight into this proton relay mechanism, we analyzed the hydrogen bonding networks for each WT trajectory. We identified three hydrogen bonding pathways that could facilitate the proton transfer reaction from the substrate to Ser215 in the WT trajectories. All of these pathways involve a water molecule near the substrate and Ser215. In the first pathway, the hydroxyl group of Ser215 is hydrogen bonded to a water molecule, which is hydrogen bonded to the carboxylate group of the substrate. In the second pathway, the hydroxyl group of Ser215 is hydrogen-bonded to a water molecule, which is hydrogen-bonded to the hydroxyl group of Thr218. In the third pathway, the first two pathways are aligned simultaneously.

Figure 4 depicts these three pathways, which are denoted the carboxylate pathway, the threonine pathway, and the dual pathway, respectively. Note that the switch between the carboxylate and threonine pathways is associated with a rotation of the hydroxyl group of Thr218. For the threonine and dual pathways, the threonine is positioned to enable proton transfer to another water molecule leading to the bulk solvent. The direct access of the hydroxyl group of Thr218 to the bulk solvent is illustrated in Figure 5. In contrast, the substrate carboxylate group was not observed to hydrogen bond to water molecules directly accessible to the bulk solvent. An advantage of the dual pathway over the threonine pathway is that the carboxylate group stabilizes the intervening water molecule. For the threonine pathway, the substrate carboxylate group may be stabilized by surrounding residues such as Lys100.

Table 1 gives the percentage of time that each pathway was observed for each of the four independent WT trajectories. The criteria used to define a hydrogen bond were a distance of less than 3.3 Å between the donor and acceptor and an angle of less than 35° between the donor-hydrogen and donor-acceptor vectors. We did not observe a significant number of switches between the different hydrogen bonding pathways during each of the 1-ns trajectories. As a result, we are unable to provide statistically meaningful probabilities or free energies of formation for each pathway.

To further characterize the differences among the hydrogen bonding pathways, we calculated the pair distribution function

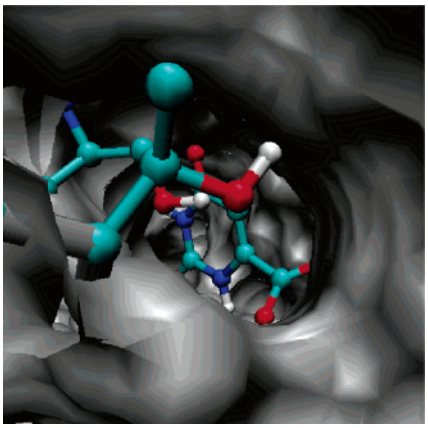

Figure 5. Illustration of the direct access of bulk solvent to the hydroxyl group of Thr218. The coordinates were obtained from the X-ray crystallographic structure for human DHOD.[3] Missing residues and hydrogen atoms were added with JACKAL.[26] The van der Waals surface created from all atoms is shown in gray. The perspective is from the exterior of the protein. Thr218 is shown in the foreground, the side chain of Ser215 is shown in the middle, and the substrate is shown in the background.

for the water molecules relative to the oxygen atom of Thr218. This pair distribution function is defined as[49,50]

$$g(r) = \frac{1}{\rho_{\text{water}}} \left\langle \sum_{i=1}^{N_{\text{water}}} \delta(r_i - r) \right\rangle \qquad (1)$$

where the summation is over the N_{water} water molecules in a sphere of radius 35 Å centered at the oxygen of Thr218, ρ_{water} is the average density of water molecules in this sphere, and r_i is the distance between the oxygen of Thr218 and the oxygen of the ith water molecule. The quantity in brackets is calculated in terms of the number density of water molecules in a spherical shell of radius r centered at the oxygen of Thr218. Thus, $g(r)$ indicates the relative density of water molecules at distance r from the oxygen of Thr218 compared to the bulk water density.

We calculated the pair distribution function $g(r)$ for two 300-ps regions of the trajectories. The first region corresponds to 96% probability of the carboxylate pathway, and the second region corresponds to 98% probability of the threonine pathway. Figure 6 depicts the results, which were found to be qualitatively similar for three different data sets for each pathway. In all cases,

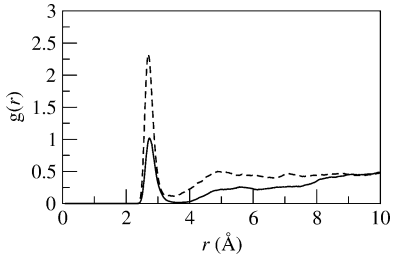

Figure 6. Pair distribution functions for the oxygen in Thr218 to the oxygens in the surrounding water molecules for the carboxylate pathway (solid) and the threonine pathway (dashed).

we verified that $g(r)$ becomes unity at large r. Note that the first peak in the pair distribution function is approximately twice as high for the threonine pathway than for the carboxylate pathway. The average number of water molecules directly hydrogen-bonded to Thr218 can be calculated by integrating over the first peak of the pair distribution function:

$$N_{\mathrm{H-bond}} = \rho_{\mathrm{water}} \int_{1\mathrm{st\ peak}} 4\pi r^2 g(r)\, \mathrm{d}r \qquad (2)$$

$N_{\mathrm{H-bond}}$ is 2.18 for the threonine pathway and 1.06 for the carboxylate pathway. This observation suggests that the hydrogen bonding pathway to Thr218 is associated with greater stabilization of Thr218 by hydrogen bonding to nearby water molecules.

We also investigated the impact of the mutation of Ser215 to cysteine on the hydrogen bonding pathways. As discussed above, in three out of the four mutant trajectories, the carboxylate group of the substrate bends toward the cysteine base, and the nearby water molecule is expelled. These structural rearrangements prevent the formation of the hydrogen bonding pathways that were observed in the WT trajectories. We observed two hydrogen bonding pathways in these mutant trajectories. In the first pathway, the thiol group of Cys215 is directly hydrogen bonded to the carboxylate of the substrate. In the second pathway, the thiol group of Cys215 is directly hydrogen bonded to Thr218.

TABLE 2: Percentage of Time That Each Hydrogen Bonding Pathway Was Observed for Each of the Four Independent Ser215Cys Mutant Trajectories[a]

	traj 1	traj 2	traj 3	traj 4
water present	2.0	0.02	100	0.00
carboxylate path	26	44	0.04	41
threonine path	1.92	1.73	0.00	1.42

[a] The mutant hydrogen bonding pathways are depicted in Figure 7. Note that these pathways involve direct hydrogen bonding between Cys215 and the carboxylate group of the substrate or Th218, and they do not involve an intervening water molecule. The percentage of time that a water molecule is present in the active site cavity, as defined in the text, is also given.

Figure 7 depicts these two hydrogen bonding pathways, and Table 2 gives the percentage of time that each pathway was observed for each of the four mutant trajectories. Note that the threonine pathway appears to be much less probable than the carboxylate pathway. For the three trajectories in which the substrate assumed the bent conformation and the nearby solvent molecule was expelled, the hydride transfer reaction from the substrate to the cofactor was inhibited because the transferring hydride was no longer oriented toward the cofactor. For the trajectory in which the substrate did not assume the bent conformation and the nearby solvent molecule was not expelled, we did not observe any hydrogen bonding pathways involving both Cys215 and this water molecule because they were too far apart. As for the WT trajectories, we were unable to obtain statistically meaningful results for the probabilities and free energies of formation of these hydrogen bonding pathways. As mentioned above, in addition to disrupting the hydrogen bonding pathways formed in the WT trajectories, the mutation of Ser215 to cysteine significantly increased the average proton and hydride donor−acceptor distances.

The pK_a of cysteine indicates that this amino acid could be deprotonated in the active site. We would expect that the electrostatic repulsion between the negatively charged thiolate and carboxylate groups would render the bent conformation of the substrate energetically unfavorable. To explore this possibility, we also performed analogous simulations with depro-

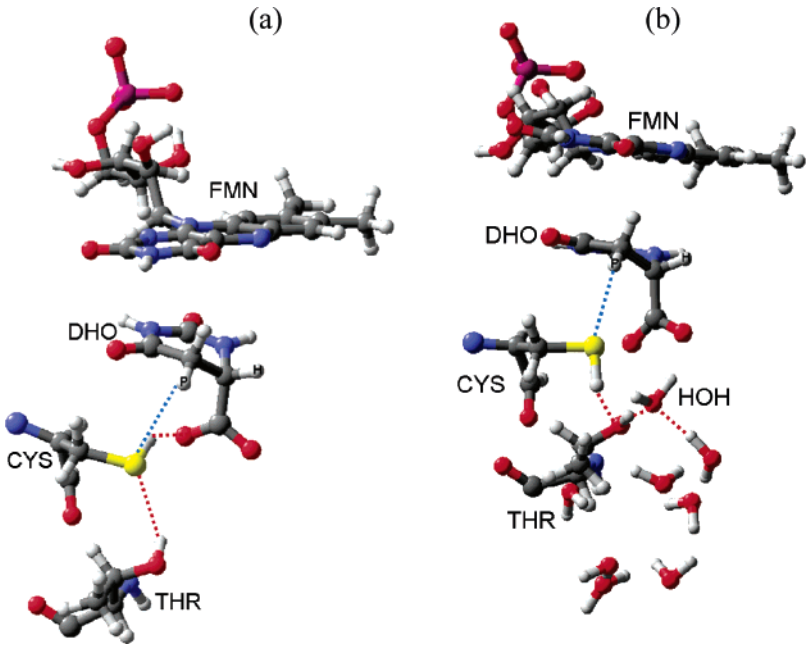

Figure 7. Hydrogen bonding pathways observed in the Ser215Cys mutant trajectories for which the intervening water molecule is expelled: (a) carboxylate pathway; (b) threonine pathway. The transferring proton is labeled as P, and the transferring hydride is labeled as H.

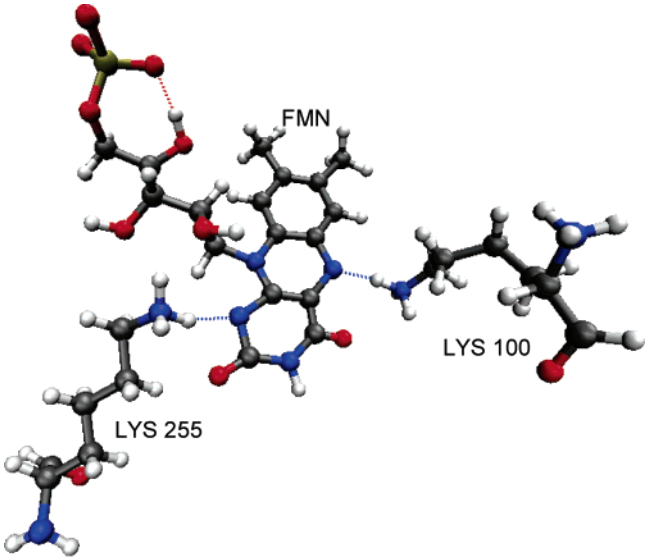

Figure 8. Hydrogen bonding of Lys100 and Lys255 to FMN for a representative configuration sampled in a WT trajectory. These hydrogen bonding interactions are maintained throughout virtually all of the trajectories.

tonated Cys215. In this case, we found that the substrate did not assume the bent conformation, but the proton donor−acceptor distance increased significantly, thereby inhibiting the proton-transfer reaction from the substrate to Cys215. These simulations indicate that the deprotonated cysteine also disrupts the hydrogen bonding network in the active site.

Residues Lys100 and Lys255 are thought to play a catalytic role in this enzyme reaction through hydrogen bonding interactions with the FMN cofactor.[1,21] Mutation of Lys100 in human DHOD has been shown experimentally to abolish enzymatic activity.[21] We analyzed the hydrogen bonding interactions of Lys100 and Lys255 to the FMN cofactor in our molecular dynamics simulations. Figure 8 illustrates these hydrogen bonding interactions for a representative configuration sampled during a WT trajectory. We found that Lys100 and Lys255 are hydrogen bonded to the FMN cofactor for at least 99% of the time in all four WT trajectories. These hydrogen bonding interactions are also observed for at least 99% of the time in three of the mutant trajectories and at least 90% of the time in the other mutant trajectory. Thus, our simulations provide support for the hypothesis that these lysine residues enhance the structural stability of the active site by hydrogen bonding to the FMN cofactor.

IV. Conclusions

In this paper, we identified and characterized potential proton relay pathways that could facilitate the redox reaction catalyzed by human DHOD. In this redox reaction, a hydride is transferred from C6 of the DHO substrate to the FMN cofactor, and a proton is transferred from C5 of the DHO substrate to a serine residue in the active site. Typically, serine does not play the role of a catalytic base. Hydrogen bonding interactions within the active site have been postulated to enhance the basicity of the active Ser215, however, and deprotonation of the substrate may involve a proton relay mechanism along a hydrogen bonding pathway in the active site.

We identified three types of hydrogen bonding pathways in the active site of WT DHOD. In the first pathway, the hydroxyl group of Ser215 is hydrogen bonded to a water molecule, which is hydrogen bonded to the carboxylate group of the substrate. In the second pathway, the hydroxyl group of Ser215 is hydrogen bonded to a water molecule, which is hydrogen bonded to the hydroxyl group of Thr218. The third pathway is a dual pathway that encompasses both of these pathways. Note that a proton relay mechanism involving the substrate carboxylate group is not consistent with experiments indicating that esters of DHO are good substrates for the bovine liver DHOD enzyme.[11,16,51] These experiments suggest that a free carboxylate anion is not necessary for the enzyme reaction. These experimental results provide support for the proton relay mechanism through Thr218. Our analysis indicated that the presence of the hydrogen bonding pathway to Thr218 is associated with greater stabilization of Thr218 by hydrogen bonding to nearby water molecules leading to the bulk solvent. An advantage of the dual hydrogen bonding pathway is that the carboxylate stabilizes the intervening water molecule that is essential for proton transfer along the pathway through Thr218 to the bulk solvent.

The mutation of Ser215 to cysteine in the related *E. coli* DHOD was found experimentally to significantly decrease the enzyme activity.[11] In general, cysteine is more reactive as a catalytic base than serine. Moreover, cysteine plays the role of the catalytic base in class 1 DHOD enzymes. To elucidate the impact of this mutation of the active base, we studied the Ser215Cys mutant human DHOD by replacing Ser215 with cysteine in our simulations. The similarity of the calculated root-mean-square fluctuations for the WT and mutant trajectories indicates that the mutation does not significantly alter the overall structure and motion of the enzyme. The average substrate proton and hydride donor−acceptor distances, however, are significantly greater in the mutant than in the WT trajectories. Furthermore, in the majority of the mutant trajectories, the water near the substrate was expelled from the active site region, and the substrate assumed a different conformation in which the carboxylate group bends toward the cysteine base. These structural rearrangements prevent the formation of the hydrogen bonding pathways that were observed in the WT trajectories and inhibit hydride transfer from the substrate to the cofactor. Alternative hydrogen bonding pathways involving direct hydrogen bonding between Cys215 and the carboxylate or, to a lesser extent, direct hydrogen bonding between Cys215 and Thr218 were observed. Even in the mutant trajectory for which the substrate maintained the WT conformation and the nearby water molecule remained, Cys215 did not form productive hydrogen bonding pathways. In simulations of the Ser215Cys mutant with a deprotonated Cys215, the substrate did not assume the bent conformation, but the hydrogen bonding network in the active site was disrupted and the proton donor−acceptor distance increased to an extent that would inhibit the proton transfer reaction.

The differences observed for the mutant DHOD trajectories may arise from the larger van der Waals radius of the sulfur atom in cysteine compared to the oxygen atom in serine. The disruption of the hydrogen bonding pathways and the greater donor−acceptor distances could lead to significant decrease in activity. The class 1 DHOD enzymes could utilize an alternative proton relay mechanism involving, for example, direct proton transfer from the cysteine base to the substrate carboxylate. For both the WT and the mutant trajectories, however, the substrate carboxylate group was not observed to hydrogen bond to water molecules directly accessible to the bulk solvent.

The inhibition of DHODs has been found to be an effective way to block pyrimidine nucleotide biosynthesis. As a result, these enzymes are promising targets for drugs treating a wide range of diseases. Thus, the elucidation of the mechanism of

DHOD is important for the design of inhibitors that selectively impact the activity of only certain members of the enzyme family. Computational studies on parasitic DHOD enzymes, as well as human DHOD, will provide additional insights for drug design.

Acknowledgment. We thank Bruce Palfey for many helpful discussions about DHOD and Kim F. Wong for useful advice about the GROMACS simulations. We are grateful for financial support from National Institutes of Health Grant GM56207 and the Alfred P. Sloan Foundation.

References and Notes

(1) Rowland, P.; Nielsen, F. S.; Jensen, K. F.; Larsen, S. *Structure* **1997**, *5*, 239.
(2) Rowland, P.; Bjornberg, O.; Nielsen, F. S.; Jensen, K. F.; Larsen, S. *Protein Sci.* **1998**, *7*, 1269.
(3) Liu, S.; Neidhardt, E. A.; Grossman, T. H.; Ocain, T.; Clardy, J. J. *Structure* **2000**, *8*, 25.
(4) Rowland, P.; Norager, S.; Jensen, K. F.; Larsen, S. *Structure* **2000**, *8*, 1227.
(5) Elliott, W. L.; Sawick, D. P.; DeFrees, S. A.; Heinstein, P. F.; Cassady, J. M.; Morre, D. J. *Biochim. Biophys. Acta* **1984**, *800*, 194.
(6) Weber, G. *Cancer Res.* **1983**, *43*, 3466.
(7) Breedveld, F. C.; Dayer, J.-M. *Ann. Rheum. Dis.* **2000**, *59*, 841.
(8) Palfey, B. A.; Bjornberg, O.; Jensen, K. F. *J. Med. Chem.* **2001**, *44*, 2861.
(9) Cherwinski, H. M.; Byars, N.; Ballaron, S. J.; Nakano, G. M.; Young, J. M.; Ransom, J. T. *Inflammation Res.* **1995**, *44*, 317.
(10) Cherwinski, H. M.; Cohn, R. G.; Cheung, P.; Webster, D. J.; Xu, Y. Z.; Caulfield, J. P.; Young, J. M.; Nakano, G. M.; Ransom, J. T. *J. Pharmacol. Exp. Ther.* **1995**, *275*, 1043.
(11) Bjornberg, O.; Gruner, A.-C.; Roepstorff, P.; Jensen, K. F. *Biochemistry* **1999**, *38*, 2899.
(12) Bjornberg, O.; Rowland, P.; Larsen, S.; Jensen, K. F. *Biochemistry* **1997**, *36*, 16197.
(13) Palfey, B. A.; Bjornberg, O.; Jensen, K. F. *Biochemistry* **2001**, *40*, 4381.
(14) Norager, S.; Jensen, K. F.; Bjornberg, O.; Larsen, S. *Structure* **2002**, *10*, 1211.
(15) Pascal, R. A., Jr.; Walsh, C. T. *Biochemistry* **1984**, *23*, 2745.
(16) Hines, V.; Johnston, M. *Biochemistry* **1989**, *28*, 1227.
(17) Argyrou, A.; Washabaugh, M. W.; Pickart, C. M. *Biochemistry* **2000**, *39*, 10373.
(18) Shi, J.; Palfey, B. A.; Dertouzos, J.; Jensen, K. F.; Gafni, A.; Steel, D. *J. Am. Chem. Soc.* **2004**, *126*, 6914.
(19) Norager, S.; Arent, S.; Bjornberg, O.; Ottosen, M.; Lo Leggio, L.; Jensen, K. F.; Larsen, S. *J. Biol. Chem.* **2003**, *278*, 28812.
(20) Hansen, M.; Le Nours, J.; Johansson, E.; Antal, T.; Ullrich, A.; Loffler, M.; Larsen, S. *Protein Sci.* **2004**, *13*, 1031.
(21) Jiang, W.; Locke, G.; Harpel, M. R.; Copeland, R. A.; Marcinkeviciene, J. *Biochemistry* **2000**, *39*, 7990.
(22) Guallar, V.; Harris, D. L.; Batista, V. S.; Miller, W. H. *J. Am. Chem. Soc.* **2002**, *124*, 1430.
(23) Lu, D.; Voth, G. A. *PROTEINS: Struct., Funct., and Genet.* **1998**, *33*, 119.
(24) Toba, S.; Colombo, G.; Merz, K. M., Jr. *J. Am. Chem. Soc.* **1999**, *121*, 2290.
(25) Cukier, R. I. *Biochim. Biophys. Acta* **2005**, *1706*, 134.
(26) Xiang, J. Z.; Honig, B. JACKAL: A Protein Structure Modeling Package; Columbia University & Howard Hughes Medical Institute: New York, 2002.
(27) IMPACT.; Schrodinger, Inc.: Portland, OR, 2000.
(28) Jorgensen, W. L.; Maxwell, D. S.; Tirado-Rives, J. *J. Am. Chem. Soc.* **1996**, *118*, 11225.
(29) QSite; Schrodinger, Inc.: Portland, OR, 2005.
(30) Murphy, R. B.; Philipp, D. M.; Friesner, R. A. *J. Comput. Chem.* **2000**, *21*, 1442.
(31) Ditchfield, R.; Hehre, W. J.; Pople, J. A. *J. Chem. Phys.* **1971**, *54*, 724.
(32) Hehre, W. J.; Ditchfield, R.; Pople, J. A. *J. Chem. Phys.* **1972**, *56*, 2257.
(33) Francl, M. M.; Pietro, W. J.; Hehre, W. J.; Binkley, J. S.; Gordon, M. S.; DeFrees, D. J.; Pople, J. A. *J. Chem. Phys.* **1982**, *77*, 3654.
(34) Lee, C.; Yang, W.; Parr, P. G. *Phys. Rev. B* **1988**, *37*, 785.
(35) Becke, A. D. *J. Chem. Phys.* **1993**, *98*, 5648.
(36) Berendsen, H. J. C.; Postma, J. P. M.; van Gunsteren, W. F.; Hermans, J. Interaction models for water in relation to protein hydration. In *Intermolecular Forces*; Pullman, B., Ed.; D. Reidel Publishing Company: Dordrecht, 1981.
(37) Breneman, C. M.; Wiberg, K. B. *J. Comput. Chem.* **1990**, *11*, 361.
(38) Chirlian, L. E.; Francl, M. M. *J. Comput. Chem.* **1987**, *8*, 894.
(39) Woods, R. J.; Khalil, M.; Pell, W.; Moffat, S. H.; Smith, V. H. *J. Comput. Chem.* **1990**, *11*, 297.
(40) Berendsen, H. J. C.; Postma, J. P. M.; van Gunsteren, W. F.; DiNola, A.; Haak, J. R. *J. Chem. Phys.* **1994**, *81*, 3684.
(41) Ewald, P. P. *Ann. Phys.* **1921**, *64*, 253.
(42) Lindahl, E.; Hess, B.; Van der Spoel, D. *J. Mol. Modelling* **2001**, *7*, 306.
(43) Berendsen, H. J. C.; Van der Spoel, D.; Van Drunen, R. *Comput. Phys. Commun.* **1995**, *91*, 43.
(44) Darden, T.; York, D.; Pedersen, L. *J. Chem. Phys.* **1993**, *98*, 10089.
(45) Schuettelkopf, A. W.; Van Aalten, D. M. F. *Acta Crystallogr.* **2004**, *D60*, 1355.
(46) Nose, S. *Mol. Phys.* **1984**, *52*, 255.
(47) Hoover, W. G. *Phys. Rev. A* **1985**, *31*, 1695.
(48) Ryckaert, J. P.; Ciccotti, G.; Berendsen, H. J. C. *J. Comput. Phys.* **1977**, *23*, 327.
(49) van der Spoel, D.; Lindahl, E.; Hess, B.; van Buuren, A. R.; Apol, E.; Meulenhoff, P. J.; Tieleman, D. P.; Sijbers, A. L. T. M.; Feenstra, K. A.; van Drunen, R.; Berendsen, H. J. C. Gromacs User Manual Version 3.2, www.gromacs.org; 2004.
(50) Allen, M. P.; Tildesley, D. J. *Computer Simulation of Liquids*; Clarendon Press: Oxford, 1989.
(51) Hines, V.; Keys, L. D., III; Johnston, M. *J. Biol. Chem.* **1986**, *261*, 1386.